ACS Macro Letters

Cite This: ACS Macro Lett. 2018, 7, 1254−1260

Letter

pubs.acs.org/macroletters

Synthesis and 3D Printing of PEG−Poly(propylene fumarate) Diblock and Triblock Copolymer Hydrogels

Rodger A. Dilla,[†] Cecilia M. M. Motta,[†] Savannah R. Snyder,[‡] James A. Wilson,[†] Chrys Wesdemiotis,[‡] and Matthew L. Becker*[,†,§]

[†]Department of Polymer Science, The University of Akron, Akron, Ohio 44325, United States

[‡]Department of Chemistry, The University of Akron, Akron, Ohio 44325, United States

[§]Department of Biomedical Engineering, The University of Akron, Akron, Ohio 44325, United States

Supporting Information

ABSTRACT: PEG-based hydrogels are used widely in exploratory tissue engineering applications but in general lack chemical and structural diversity. Additive manufacturing offers pathways to otherwise unattainable scaffold morphologies but has been applied sparingly to cross-linked hydrogels. Herein, monomethyl ether poly(ethylene glycol) (PEG) and PEG−diol were used to initiate the ring-opening copolymerization (ROCOP) of maleic anhydride and propylene oxide to yield well-defined diblock and triblock copolymers of PEG−poly(propylene maleate) (PPM) and ultimately PEG-poly(propylene fumarate) (PPF) with different molecular mass PEG macroinitiators and block length ratios. Using continuous digital light processing (cDLP), hydrogels were photochemically printed from an aqueous solution which resulted in a 10-fold increase in elongation at break compared to traditional diethyl fumarate (DEF) based printing. Furthermore, PPF−PEG−PPF triblock hydrogels were also found to be biocompatible *in vitro* across a number of engineered MC3T3, NIH3T3, and primary Schwann cells.

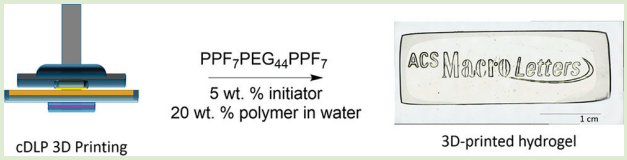

Synthetic hydrogels, while used widely for a number of tissue engineering applications, are limited in the number and type of chemical groups used for network formation and structural elements that can be used to manipulate the network structure.[1,2] Furthermore, they generally require several criteria to be clinically relevant. In addition to maintaining cell viability, a combination of suitable mechanical properties with sufficient processing flexibility to yield morphologically and structurally complex scaffolds is desirable.[3] A number of reports have demonstrated that both mechanical properties as well as scaffold topology significantly influence cell proliferation, migration, and differentiation; therefore, a functional material should concomitantly mimic the mechanical properties of the target tissue while providing a processing handle to produce complex, high-resolution structures.[4−20]

Hydrogels are networks of hydrophilic polymers that can be tailored to match a broad range of design parameters as a consequence of their tunable mechanical properties and intrinsic network morphology.[21] For example, the modulus of poly(ethylene glycol) (PEG) oxime hydrogels can be tuned using a kinetically controlled cross-linking reaction independent of chemistry, concentration, and stoichiometry.[22] The moduli of other hydrogel systems can be adjusted by changing the weight percent of the hydrogel.[23] Furthermore, functionalization of hydrogels has afforded investigations into the role of exogenous bioactive ligands on cell behavior.[20,24,25] Microfabrication techniques such as microcontact printing, templated photolithography, and microfluidic molding have each afforded access to micrometer- and nanometer-sized structures.[26] However, many hydrogel systems are limited to casting fabrication techniques, greatly limiting the variety as well as resolution control of scaffold architectures that can be produced.

Additive manufacturing has provided avenues to morphologically complex structures unachievable by other processing methods.[27] This technique provides a number of advantages in the development of tissue engineering scaffolds as features such as porosity and increased surface area promote host infiltration within a synthetic implant.[28] Additive manufacturing modalities such as fused deposition modeling (FDM) have been applied to hyaluronic acid and sodium alginate-based gels.[29] Furthermore, a recent report demonstrated the use of continuous digital light processing (cDLP) to print PEG−diacrylate (PEG-DA) hydrogels into high-resolution structures.[30] cDLP methods use the stepwise production of UV-cured layers to build a structure from a photoreactive liquid resin.[31] This technique can produce extremely fine (e.g., <120 μm) features and through the use of computer-aided modeling (CAM) can be tailored to create scaffolds for patient-specific defects.[32] However, the viscosity of the polymer resin must be sufficiently low that it can flow readily (e.g., $\eta^* \leq 1-3$ Pa s), requiring the use of a solvent or diluent for many polymers.

Received: September 19, 2018
Accepted: September 24, 2018
Published: October 1, 2018

DOI: 10.1021/acsmacrolett.8b00720
ACS Macro Lett. 2018, 7, 1254−1260

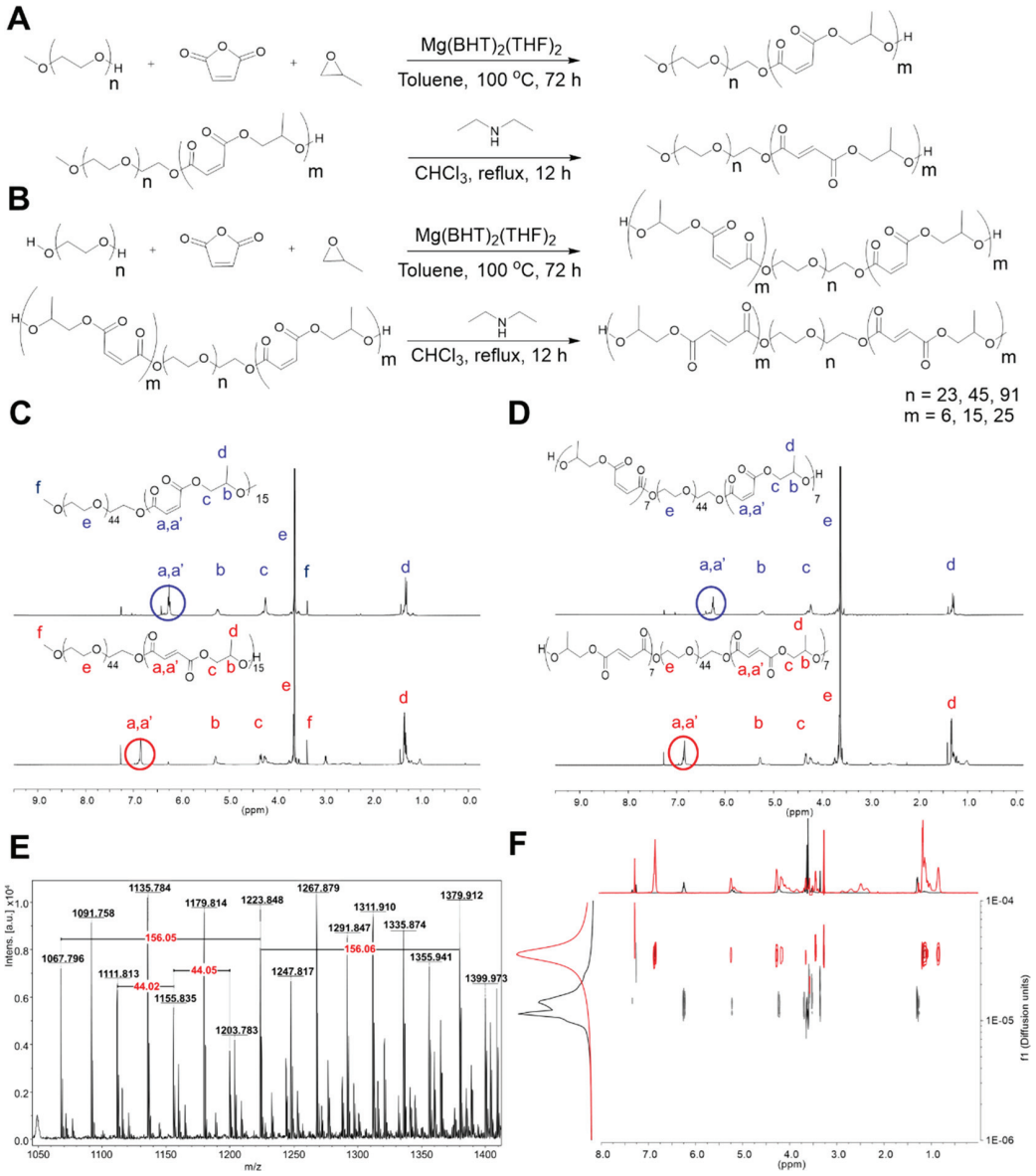

Figure 1. Synthesis of PEGPPF di- and triblock copolymers initiated by (A) methyl ether PEG to produce poly(ethylene glycol-*b*-propylene maleate) and (B) PEG−diol to produce poly(propylene maleate-*b*-ethylene glycol-*b*-propylene maleate). (C) Isomerization using diethylamine as a catalyst yielded the poly(ethylene glycol-*b*-propylene fumarate) and (D) poly(propylene fumarate-*b*-ethylene glycol-*b*-propylene fumarate) products. (E) MALDI-TOF spectrum of poly(propylene fumarate-*b*-ethylene glycol-*b*-propylene fumarate). (F) Diffusion-ordered NMR spectroscopy (DOSY-NMR) spectra of poly(ethylene glycol-*b*-propylene fumarate) block copolymer (red line) and the homopolymer mixture of methyl ether PEG and PPM (black line).

One such polymer that has shown great utility for cDLP is poly(propylene fumarate) (PPF), a degradable, unsaturated polyester. First reported by Mikos and co-workers and developed specifically for bone tissue regeneration, this UV-cross-linkable polymer provides robust mechanical strength while also degrading into a Krebs-cycle constituent (fumaric acid) and a ubiquitous food additive (propylene glycol).[33] While the first described syntheses utilized step-growth polymerizations, Coates and co-workers demonstrated the ring-opening copolymerization (ROCOP) of propylene oxide (PO) and maleic anhydride (MA) in the presence of a cobalt catalyst to produce well-controlled PPM that could be converted to PPF upon isomerization.[34] Producing narrow molecular mass distribution polymers can be useful in regenerative medicine applications as chain length and distribution can affect degradation, mechanical properties, and the fidelity of the scaffold structure.[35−37] Magnesium ethoxide has since been utilized as a ROCOP catalyst to produce PPF albeit with less control but avoiding the toxicity of cobalt. With the use of diethyl fumarate (DEF) as a viscosity modifier and reactive diluent, PPF was formed into cell-viable scaffolds using cDLP.[27] Finally, a recent report further demonstrated the well-controlled ROCOP of PPF using $Mg(BHT)_2(THF)_2$ as a catalyst, resulting in molecular mass distributions ($Đ_m$) similar to those reported by Coates and co-workers.[38] Furthermore, chain-end functionalization was achieved in this system using a functional alcohol initiator,

DOI: 10.1021/acsmacrolett.8b00720
ACS Macro Lett. 2018, 7, 1254−1260

Table 1. Synthesis of PEGPPF Diblock and Triblock Copolymers

entry	PEG initiator[a]	target DP PPF[b]	temperature (°C)	time (days)	MA conversion (%)	M_n[c] (kDa)	M_n[d] (kDa)	M_w[d] (kDa)	$Đ_M$[d]
1	m 1000	6	100	3	94	1.9	2.4	3.7	1.59
2	m 1000	15	100	4	75	2.6	2.2	3.4	1.55
3	m 1000	25	100	5	91	3.5	1.6	2.2	1.38
4	m 2000	6	100	3	94	3.0	1.6	2.0	1.25
5	m 2000	15	100	4	83	4.6	2.6	4.5	1.70
6	m 2000	25	100	5	70	5.1	2.6	3.1	1.31
7	m 4000	6	100	3	93	5.1	5.2	7.0	1.36
8	m 4000	15	100	4	93	6.6	2.1	4.3	1.49
9	m 4000	25	100	5	94	7.0	3.9	4.4	1.12
10	d 1000	6	100	3	88	-	4.4	7.2	1.65
11	d 1000	15	100	4	94	-	2.6	2.9	1.11
12	d 1000	25	100	5	95	-	3.9	6.2	1.57
13	d 2000	6	100	3	93	-	0.5	0.5	1.12
14	d 2000	15	100	4	95	-	3.6	4.9	1.49
15	d 2000	25	100	5	97	-	4.6	7.5	1.61
16	d 4000	6	100	3	91	-	4.3	7.2	1.65
17	d 4000	15	100	4	99	-	6.7	10.0	1.51
18	d 4000	25	100	5	94	-	4.3	8.3	1.92

[a]Where m = methyl ether PEG, d = PEG−diol, and values indicates molecular mass (Da). [b]Based on an initiator-to-monomer ratio. [c]Based on end-group analysis using ^{1}H NMR spectroscopy. [d]Based on SEC against poly(styrene) standards

simultaneously introducing a reactive handle for postpolymerization and postprinting functionalization.

The facile ROCOP initiation of PPF using a number of primary alcohols led to the notion of polymerizing PPF from the end of a PEG−diol chain to produce robust, 3D-printable hydrogel precursors. Multiblock poly(propylene fumarate-*co*-ethylene glycol) with broad molecular mass distributions were reported previously by Suggs et al., employing a step-growth polymerization followed by a transesterification mechanism to incorporate ethylene glycol subunits into PPF.[39] In contrast, this paper seeks to present the formation of well-ordered block copolymers of PEG_nPPF_m and $PPF_mPEG_nPPF_m$ utilizing the magnesium-based catalyst. Formation of hydrogels by photo-cross-linking will be explored, in the context of both casting and 3D-printing by cDLP, as well as the resultant swelling and tensile mechanical properties.

Poly(propylene maleate) (PPM) was formed from the alternating ROCOP of MA and PO in the presence of $Mg(BHT)_2(THF)_2$ catalyst, initiated from the alcohol chain end of both methyl ether PEG and PEG−diol to form diblock (PEG_nPPM_m) and triblock ($PPM_mPEG_nPPM_m$) copolymers (Figure 1A and B) (Table 1), respectively. Using a molar ratio of 1:5 (catalyst:initiator), polymerizations exceeded 90% conversion in all cases except for entries **2** and **6** as determined by integration of the residual maleic anhydride peak in ^{1}H NMR spectroscopy. The lower conversions can be attributed to larger head space in the reaction vessel: PO boils at 34 °C and must be condensed back into solution. It was experimentally determined that by minimizing this head space the reactions are driven to higher conversion. The polymers were then isomerized to the PEG_nPPF_m and $PPF_mPEG_nPPF_m$ species by treatment with diethylamine (Figure 1C and D). The final polymer products were characterized by MALDI-TOF mass spectrometry to show the PPF repeat unit of 156 Da and the PEG repeat unit of 44 Da (Figure 1E). The final molar mass distributions of the diblock copolymers (Table 1, entries 1−9) were calculated via end group analysis from ^{1}H NMR and size exclusion chromatography (SEC), while the triblock copolymers were analyzed by SEC as a consequence of potentially identical end groups (i.e., no terminal methyl group for analysis, and end groups could be MA on either chain end, PO group on either chain end, or a combination of the aforementioned). In this case, the end group analysis via ^{1}H NMR spectroscopy demonstrated a consistent increase in number-average molecular weight (M_n) with targeted degree of polymerization, indicating the successful synthesis of blocks of varying lengths. Comparatively, the SEC data did not display such a linear increase of molecular mass with increasing block length. However, this can be attributed to the use of poly(styrene) standards, whose hydrodynamic radii in tetrahydrofuran (THF) solvent are expected to be much different than that of the block copolymers and the relatively low molecular mass.

To demonstrate that well-defined block copolymers had been synthesized, diffusion-ordered NMR spectroscopy (DOSY-NMR) and quantitative ^{13}C NMR spectroscopy experiments were employed. An example DOSY-NMR spectrum displays separate diffusional bands in a mixture of the two homopolymers compared to the block copolymer itself (Figure 1F). Furthermore, in the ^{13}C NMR spectra, the carbonyl diad resonances of the PPF repeat unit (δ = 164.4 and 164.0 ppm) are split by PEG carbons adjacent to them. As the integration values of the carbonyl PPF peaks adjacent to PEG are lower than those adjacent to PPF, it stands to reason that a sharp interface between the two blocks exists. This can also be observed from the PEG carbonyl diad resonance (δ = 70.55 ppm) which is split by the PPF block interface (Figure S1).

cDLP additive manufacturing involves cross-linking a photoreactive polymer resin into a solid using ultraviolet light. This technique requires sufficiently low resin viscosities (i.e., <3 Pa s) to allow the polymer to flow into the void space as the printed product is raised out of the resin. The resin form of pure $PPF_3PEG_{23}PPF_3$ block copolymer has a complex viscosity of about 35−50 Pa s measured by small-angle oscillatory shear (SAOS) rheology. These values are far too viscous for this manufacturing method and therefore must be diluted. Dean and co-workers have shown that DEF is well

DOI: 10.1021/acsmacrolett.8b00720
ACS Macro Lett. 2018, 7, 1254−1260

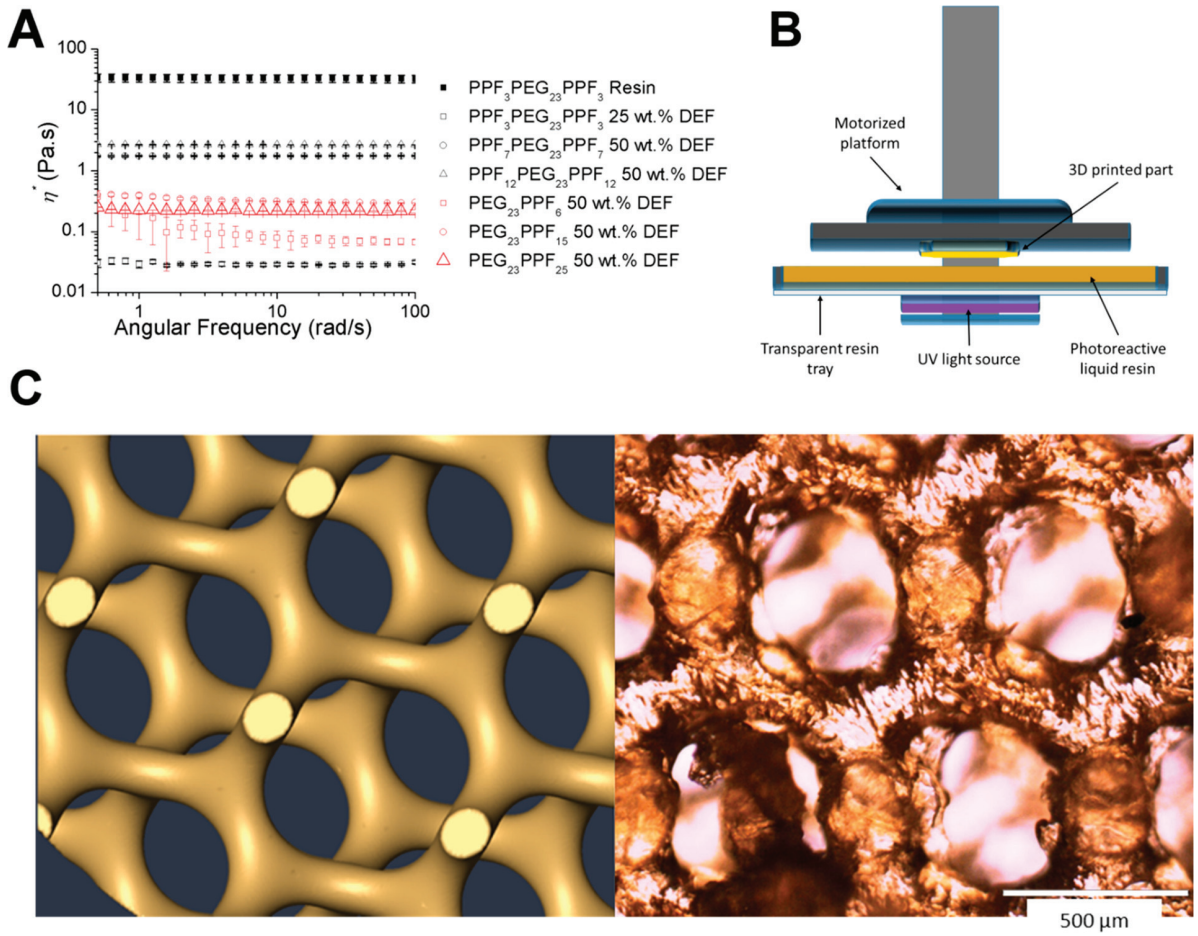

Figure 2. Viscometry and cDLP printing of $PPF_mPEG_{23}PPF_m$ with DEF. (A) DEF was used as a viscosity modifier for the extremely viscous homopolymer resin, 50 wt % being found optimal for 3D printing. (B) cDLP printing schematic. (C) A CAD model of a gyroidal scaffold (left) was successfully printed from a 50 wt % solution of $PPF_3PEG_{23}PPF_3$ in DEF.

suited for this purpose as a solution with a 1:1 ratio of polymer:DEF easily produces a usable viscosity (<1 Pa s) for homopolymer PPF.[31] Similarly, 3:1 and 1:1 ratios of DEF:$PPF_mPEG_nPPF_m$ yielded viscosities <3 Pa s for all variants of $PPF_mPEG_{23}PPF_m$ as well as $PEG_{23}PPF_m$ (Figure 2A).

For cDLP printing with DEF-resin, $PPF_mPEG_{23}PPF_m$ (i.e., 1 kDa PEG) triblock copolymers were successfully printed using a 1:1 mass ratio of polymer:DEF. A printing formulation previously developed by Dean et al. was added: 3 wt % BAPO, an acylphosphine photoinitiator, 0.4% Irgacure 784, a titanocene-based initiator/light scattering agent, and 0.7% oxybenzone, a radical scavenger.[31] To demonstrate the print resolution of $PPF_3PEG_{23}PPF_3$ polymer, a gyroidal scaffold with strut sizes ~100 μm in diameter was printed from a computer-generated model (Figure 2C). An optical image of the printed structure demonstrates the high resolution of $PPF_3PEG_{23}PPF_3$ from cDLP printing.

During cDLP printing in aqueous solution for tested $PPF_mPEG_nPPF_m$ species with PEG block >1000 Da, the polymers are insoluble in DEF, limiting its use as a viscosity modifier. Fortuitously, above a PEG block mass of 2000 Da (i.e., PEG_{45} and PEG_{91}) the polymers become water soluble and when dissolved yield usable viscosities for cDLP printing, which requires sufficiently low viscosity in which the resin can flow (e.g., typically $\eta^* \leq 3$ Pa s) (Figure 3A). This provides a 2-fold advantage over previously utilized PPF:DEF mixtures by simultaneously achieving usable viscosities as well as removing the need for DEF, which as a reactive diluent is incorporated into printed scaffolds and therefore changes the material properties.

One challenge with cDLP is selecting a photoinitiator for a printing formulation. To cross-link the water-soluble polymers, the photoinitiator lithium acylphosphinate (LAP) was used.[40] In addition to water solubility, LAP also has a much higher molar absorptivity coefficient when compared to the widely used Irgacure 2959 (in the range of 340−420 nm). Furthermore, it is also cytocompatible making it an ideal photoinitiator for cross-linking water-soluble PEGPPF.[41] As the printer emits light at 405 nm this combination of properties made LAP an ideal choice to attempt cDLP printing from an aqueous solution, which proved fruitful in the successful printing of $PPF_3PEG_{45}PPF_3$.

For PEG−PPF hydrogels, the water-soluble species of $PPF_mPEG_nPPF_m$ (i.e., PEG_{45} and PEG_{91} blocks) were photo-cross-linked into hydrogels to examine their swelling properties and cell viability. Each gel was cast at 25 wt % in water with a 5:1 molar ratio of reactive center (double bond):LAP to ensure uniform cross-linking. The swelling of $PPF_mPEG_{91}PPF_m$ (i.e., 4 kDa PEG) (Q, eq S1) species is much higher than

DOI: 10.1021/acsmacrolett.8b00720
ACS Macro Lett. 2018, 7, 1254−1260

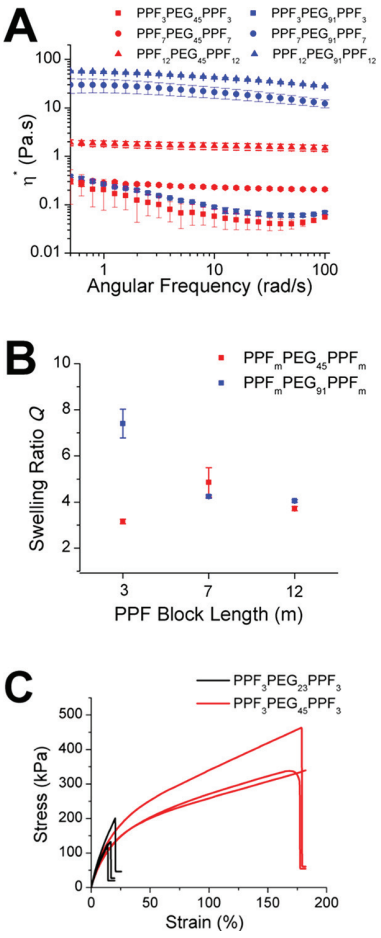

Figure 3. $PPF_mPEG_nPPF_m$ hydrogels. (A) The water solubility of $PPF_mPEG_nPPF_m$ copolymers with PEG > 2000 Da produces suitable viscosities for cDLP at ∼25 wt %. (B) Swelling ratios of $PPF_mPEG_nPPF_m$ hydrogels. (C) Stress−strain curves for water-printed $PPF_3PEG_{45}PPF_3$ and DEF-printed $PPF_3PEG_{23}PPF_3$ tensile bars.

$PPF_mPEG_{45}PPF_m$ for short PPF block lengths but quickly converges as the PPF block length increases (Figure 3B). This is a consequence of the increasing quantity of cross-linking sites which decrease the distance between cross-links and suppress swelling of the scaffold. Furthermore, the PPF block length increases concomitantly with hydrophobicity, which promotes the aggregation of the reactive centers compared to the shorter chains and potentially increases the number of cross-links formed. Finally, to assess the impact of the sterilization process for cell viability assays (i.e., incubation in ethanol followed by autoclaving) the swelling properties of cast hydrogels were measured following sterilization (Figure S11). The increased swelling ratios compared to unsterilized gels indicate that some degradation is occurring. This effect is most pronounced for the shortest PPF block lengths ($m = 3$) as the cross-link density is lowest in those materials, while the longer PPF blocks did not change as drastically. While the gels remained intact enough for cell viability assays, this indicates a softer sterilization method such as e-beam methods will be needed for clinical translation.

Now we discuss the tensile properties of 3D-printed $PPF_mPEG_nPPF_m$ hydrogels. 3D-printing from an aqueous solution yielded distinctly different mechanical properties compared to printing from a DEF-based resin. The tensile properties of water-printed $PPF_3PEG_{45}PPF_3$ material demonstrated a 10-fold increase in strain at break compared to DEF-printed $PPF_3PEG_{23}PPF_3$ (Figure 3C). This extension can be attributed to the lack of DEF, thereby producing a network with greater distance between cross-links. In the case of $PPF_3PEG_{23}PPF_3$, DEF is incorporated into the final network and produces a highly cross-linked and somewhat brittle material. In contrast, the lower cross-linking density in the water-printed hydrogel affords a notable increase in conformational relaxation modes of the PEG chains allowing them to extend farther before material failure. Surprisingly, the moduli of the two conditions were similar ($PPF_3PEG_{45}PPF_3$: 9.1 ± 0.1 kPa; $PPF_3PEG_{23}PPF_3$: 8.9 ± 0.1 kPa), indicating the extension at break can be tuned independently of modulus.

The potential of $PPF_mPEG_nPPF_m$ ($n = 45, 91$) hydrogels for use in soft tissue applications, such as peripheral nerve regeneration, was evaluated using a viability assay with three different cell types. Mouse preosteoblast MC3T3-E1 cells have been frequently used for elucidating baseline cell responses for orthopedic materials. Schwann cells are the principal glia that support neurons in the peripheral nervous system, and NIH 3T3 are a commonly used fibroblast cell line.[42−44] Not surprisingly, after 24 h of cell culture the dominant green fluorescence from live cells demonstrated that $PPF_mPEG_nPPF_m$ hydrogels have high viability when each of the cell types was cultured on sterile disks of the cross-linked samples (Figure 4).

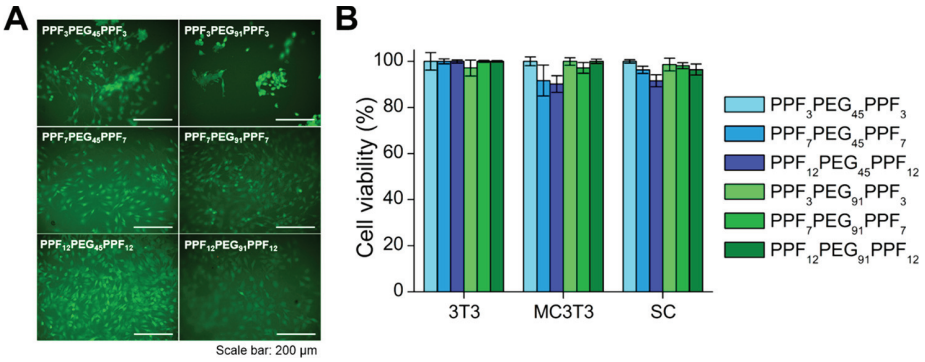

Figure 4. Viability of various engineered and primary cell lines on $PPF_mPEG_nPPF_m$ hydrogels. (A) Representative fluorescent images of primary Schwann cells stained with Calcein AM (green, live cells) and ethidium bromide (red, dead cells). (B) The viability of NIH3T3, MC3T3, and Schwann cells normalized to glass slide controls was nearly quantitative.

DOI: 10.1021/acsmacrolett.8b00720
ACS Macro Lett. 2018, 7, 1254−1260

These results indicate that the materials are nontoxic and exhibit compatibility with each of the three cell types. This was ideal as it promotes the potential for $PPF_mPEG_nPPF_m$ as a biomaterial to become translationally relevant in a number of diverse applications.

Further exploration of cellular response can be achieved by tethering bioactive ligands. This could be achieved through the incorporation of functionalized epoxide monomers such as glycidyl propargyl ether for azide−alkyne cycloadditions or by performing thiol−ene additions to unreacted double bonds in the backbone, the latter of which has been shown to exist post-cross-linking.[45,46] Through orthogonal chemical approaches, multiple peptide sequences could be tethered to the same scaffold.

The availability and diversity of printable and resorbable materials will be critical to using additive manufacturing in regenerative medicine. Using a magnesium catalyst, PPF was successfully synthesized by ROCOP from the chain end of both methyl ether PEG and PEG−diol to produce a series of PEG_nPPF_m diblock and $PPF_mPEG_nPPF_m$ triblock copolymers, respectively. Hydrogels printed in aqueous conditions demonstrated a noticeable increase in elongation at break compared to a DEF-printed variant. Additionally, the ability to manipulate strain at break independent of modulus was demonstrated. Finally, $PPF_mPEG_nPPF_m$ (n = 45, 91) hydrogels were found to be compatible with MC3T3, NIH3T3, and Schwann cell lines demonstrating the potential of these materials in tissue-engineering applications. While this report constitutes only an initial demonstration, we are exploring many more specific applications of these materials across regenerative medicine and nanomedicine.

■ ASSOCIATED CONTENT

Supporting Information

The Supporting Information is available free of charge on the ACS Publications website at DOI: 10.1021/acsmacrolett.8b00720.

Complete experimental details including materials, initiators, monomer, and polymer synthesis, isomerization conditions, and characterization of all polymers by ^{1}H NMR, ^{13}C NMR, size exclusion chromatography, and rheology conditions. Also included are model prints and cell viability images for the various formulations and cell types (PDF)

■ AUTHOR INFORMATION

Corresponding Author

*Phone: (330) 972-2834. E-mail: becker@uakron.edu.

ORCID

Chrys Wesdemiotis: 0000-0002-7916-4782

Matthew L. Becker: 0000-0003-4089-6916

Notes

The authors declare the following competing financial interest(s): The authors have submitted a PCT patent application to the USPTO. The PCT has been licensed to 21st Century Medical Technologies (21MedTech). ML Becker is a founder, board member and equity holder in 21MedTech.

■ ACKNOWLEDGMENTS

The authors gratefully acknowledge financial support from RESBIO "Integrated Technology Resource for Polymeric Biomaterials" (NIH-NIBIB & NCMHD P41EB001046), the National Science Foundation (CHE-1808115), and the W. Gerald Austen Endowed Chair in Polymer Science and Polymer Engineering via the John S. and James L. Knight Foundation.

■ REFERENCES

(1) Zhu, J.; Marchant, R. E. Design Properties of Hydrogel Tissue-Engineering Scaffolds. *Expert Rev. Med. Devices* **2011**, *8* (5), 607−626.

(2) Lampe, K. J.; Antaris, A. L.; Heilshorn, S. C. Design of Three-Dimensional Engineered Protein Hydrogels for Tailored Control of Neurite Growth. *Acta Biomater.* **2013**, *9* (3), 5590−5599.

(3) Neves, L. S.; Rodrigues, M. T.; Reis, R. L.; Gomes, M. E. Current Approaches and Future Perspectives on Strategies for the Development of Personalized Tissue Engineering Therapies. *Expert Rev. Precis. Med. Drug Dev.* **2016**, *1* (1), 93−108.

(4) Engler, A. J.; Sen, S.; Sweeney, H. L.; Discher, D. E. Matrix Elasticity Directs Stem Cell Lineage Specification. *Cell* **2006**, *126* (4), 677−689.

(5) Discher, D. E.; Janmey, P.; Wang, Y. Tissue Cells Feel and Respond to the Stiffness of Their Substrate. *Science* **2005**, *310* (5751), 1139−1143.

(6) McBeath, R.; Pirone, D. M.; Nelson, C. M.; Bhadriraju, K.; Chen, C. S. Cell Shape, Cytoskeletal Tension, and RhoA Regulate Stem Cell Lineage Commitment. *Dev. Cell* **2004**, *6* (4), 483−495.

(7) Dalby, M. J.; Gadegaard, N.; Tare, R.; Andar, A.; Riehle, M. O.; Herzyk, P.; Wilkinson, C. D. W.; Oreffo, R. O. C. The Control of Human Mesenchymal Cell Differentiation Using Nanoscale Symmetry and Disorder. *Nat. Mater.* **2007**, *6*, 997−1003.

(8) Wang, G.; Ao, Q.; Gong, K.; Wang, A.; Zheng, L.; Gong, Y.; Zhang, X. The Effect of Topology of Chitosan Biomaterials on the Differentiation and Proliferation of Neural Stem Cells. *Acta Biomater.* **2010**, *6* (9), 3630−3639.

(9) Benitez, P. L.; Mascharak, S.; Proctor, A. C.; Heilshorn, S. Use of Protein-Engineered Fabrics to Identify Design Rules for Integrin Ligand Clustering in Biomaterials. *Integr. Biol.* **2015**, *8*, 50−61.

(10) Baker, B. M.; Trappmann, B.; Wang, W. Y.; Sakar, M. S.; Kim, I. L.; Shenoy, V. B.; Burdick, J. a.; Chen, C. S. Cell-Mediated Fibre Recruitment Drives Extracellular Matrix Mechanosensing in Engineered Fibrillar Microenvironments. *Nat. Mater.* **2015**, *14* (12), 1262−1268.

(11) Clark, P. The Effects of Topographic and Mechanical-Properties of Materials on Cell Behavior. *Crit. Rev. Biocompat.* **1990**, *5* (4), 343−362.

(12) Storm, C.; et al. Nonlinear Elasticity in Biological Gels. *Nature* **2005**, *435*, 191−194.

(13) Young, D. A.; Choi, Y. S.; Engler, A. J.; Christman, K. L. Stimulation of Adipogenesis of Adult Adipose-Derived Stem Cells Using Substrates That Mimic the Stiffness of Adipose Tissue. *Biomaterials* **2013**, *34* (34), 8581−8588.

(14) Choi, Y. S.; Vincent, L. G.; Lee, A. R.; Dobke, M. K.; Engler, A. J. Mechanical Derivation of Functional Myotubes from Adipose-Derived Stem Cells. *Biomaterials* **2012**, *33* (8), 2482−2491.

(15) Reilly, G. C.; Engler, A. J. Intrinsic Extracellular Matrix Properties Regulate Stem Cell Differentiation. *J. Biomech.* **2010**, *43* (1), 55−62.

(16) Wen, J. H.; Vincent, L. G.; Fuhrmann, A.; Choi, Y. S.; Hribar, K. C.; Taylor-Weiner, H.; Chen, S.; Engler, A. J. Interplay of Matrix Stiffness and Protein Tethering in Stem Cell Differentiation. *Nat. Mater.* **2014**, *13*, 979−987.

(17) Murphy, W. L.; McDevitt, T. C.; Engler, A. J. Materials as Stem Cell Regulators. *Nat. Mater.* **2014**, *13* (6), 547−557.

(18) Tanaka, M.; Takayama, A.; Ito, E.; Sunami, H.; Yamamoto, S.; Shimomura, M. Effect of Pore Size of Self-Organized Honeycomb-Patterned Polymer Films on Spreading, Focal Adhesion, Proliferation, and Function of Endothelial Cells. *J. Nanosci. Nanotechnol.* **2007**, *7* (3), 763−772.

DOI: 10.1021/acsmacrolett.8b00720
ACS Macro Lett. 2018, 7, 1254−1260

(19) Levental, I.; Georges, C.; Janmey, P. A. Soft Biological Materials and Their Impact on Cell Function. *Soft Matter* **2007**, *3*, 299−306.
(20) Khetan, S.; Guvendiren, M.; Legant, W. R.; Cohen, D. M.; Chen, C. S.; Burdick, J. a. Degradation-Mediated Cellular Traction Directs Stem Cell Fate in Covalently Crosslinked Three-Dimensional Hydrogels. *Nat. Mater.* **2013**, *12* (5), 458−465.
(21) Lin, F.; Yu, J.; Tang, W.; Zheng, J.; Defante, A.; Guo, K.; Wesdemiotis, C.; Becker, M. L. Peptide-Functionalized Oxime Hydrogels with Tunable Mechanical Properties and Gelation Behavior. *Biomacromolecules* **2013**, *14* (10), 3749−3758.
(22) Zander, Z. K.; Hua, G.; Wiener, C. G.; Vogt, B. D.; Becker, M. L. Control of Mesh Size and Modulus by Kinetically Dependent Cross-Linking in Hydrogels. *Adv. Mater.* **2015**, *27* (40), 6283−6288.
(23) Denisin, A. K.; Pruitt, B. L. Tuning the Range of Polyacrylamide Gel Stiffness for Mechanobiology Applications. *ACS Appl. Mater. Interfaces* **2016**, *8*, 21893−21902.
(24) DeForest, C. A.; Anseth, K. S. Cytocompatible Click-Based Hydrogels with Dynamically Tunable Properties through Orthogonal Photoconjugation and Photocleavage Reactions. *Nat. Chem.* **2011**, *3* (12), 925−931.
(25) Cosgrove, B. D.; Mui, K. L.; Driscoll, T. P.; Caliari, S. R.; Mehta, K. D.; Assoian, R. K.; Burdick, J. A.; Mauck, R. L. N-Cadherin Adhesive Interactions Modulate Matrix Mechanosensing and Fate Commitment of Mesenchymal Stem Cells. *Nat. Mater.* **2016**, *15*, 1297−1306.
(26) Yanagawa, F.; Sugiura, S.; Kanamori, T. Hydrogel Microfabrication Technology toward Three Dimensional Tissue Engineering. *Regen. Ther.* **2016**, *3*, 45−57.
(27) Luo, Y.; Dolder, C. K.; Walker, J. M.; Mishra, R.; Dean, D.; Becker, M. L. Synthesis and Biological Evaluation of Well-Defined Poly(Propylene Fumarate) Oligomers and Their Use in 3D Printed Scaffolds. *Biomacromolecules* **2016**, *17* (2), 690−697.
(28) Hollister, S. J. Porous Scaffold Design for Tissue Engineering. *Nat. Mater.* **2005**, *4*, 518−524.
(29) He, Y.; Yang, F.; Zhao, H.; Gao, Q.; Xia, B.; Fu, J. Research on the Printability of Hydrogels in 3D Bioprinting. *Sci. Rep.* **2016**, *6*, 29977.
(30) Wang, J.; Altun, A. A.; Stanic, S.; Schwentenwein, M.; Jin, L.; Dietliker, K.; et al. A Highly Efficient Waterborne Photoinitiator for Visible-Light-Induced Three- Dimensional Printing of Hydrogels. *Chem. Commun.* **2018**, *54*, 920−923.
(31) Dean, D.; Jonathan, W.; Siblani, A.; Wang, M. O.; Kim, K.; Mikos, A. G.; Fisher, J. P. Continuous Digital Light Processing (CDLP): Highly Accurate Additive Manufacturing of Tissue Engineered Bone Scaffolds. *Virtual Phys. Prototyp.* **2012**, *7* (1), 13−24.
(32) Cheah, C.; Ph, D.; Chua, C.; Cheong, C.-H.; Naing, M.-w. Automatic Algorithm for Generating Complex Polyhedral Scaffold Structures for Tissue Engineering. *Tissue Eng.* **2004**, *10* (3), 595−610.
(33) Yaszemski, M. J.; Payne, R. G.; Hayes, W. C.; Langer, R. S.; Aufdemorte, T. B.; Mikos, A. G. The Ingrowth of New Bone Tissue and Initial Mechanical Properties of a Degrading Polymeric Composite Scaffold. *Tissue Eng.* **1995**, *1* (1), 41−52.
(34) Diciccio, A. M.; Coates, G. W. Ring-Opening Copolymerization of Maleic Anhydride with Epoxides: A Chain-Growth Approach to Unsaturated Polyesters. *J. Am. Chem. Soc.* **2011**, *133*, 10724−10727.
(35) Walker, J. M.; Bodamer, E.; Krebs, O.; Luo, Y.; Kleinfehn, A.; Becker, M. L.; Dean, D. Effect of Chemical and Physical Properties on the In Vitro Degradation of 3D Printed High Resolution Poly-(Propylene Fumarate) Scaffolds. *Biomacromolecules* **2017**, *18* (4), 1419−1425.
(36) Capasso Palmiero, U.; Maraldi, M.; Manfredini, N.; Moscatelli, D. Zwitterionic Polyester-Based Nanoparticles with Tunable Size, Polymer Molecular Weight, and Degradation Time. *Biomacromolecules* **2018**, *19* (4), 1314−1323.
(37) Hirschberg, V.; Schwab, L.; Cziep, M.; Wilhelm, M.; Rodrigue, D. Influence of Molecular Properties on the Mechanical Fatigue of Polystyrene (PS) Analyzed via Wöhler Curves and Fourier Transform Rheology. *Polymer* **2018**, *138*, 1−7.
(38) Wilson, J. A.; Luong, D.; Kleinfehn, A. P.; Sallam, S.; Wesdemiotis, C.; Becker, M. L. Magnesium Catalyzed Polymerization of End Functionalized Poly(Propylene Maleate) and Poly(Propylene Fumarate) for 3D Printing of Bioactive Scaffolds. *J. Am. Chem. Soc.* **2018**, *140*, 277−284.
(39) Suggs, L. J.; Krishnan, R. S.; Garcia, C. A.; Peter, S. J.; Anderson, J. M.; Mikos, A. G. Vitro and in Vivo Degradation of Poly(Propylene Fumarate-Co-Ethylene Glycol) Hydrogels. *J. Biomed. Mater. Res.* **1998**, *42*, 312−320.
(40) Majima, E.; Schnabel, W.; Weber, W. Phenyl-2,4,6-Trimethylbenzoylphosphinates as Water Soluble Photoinitiators. Generation and Reactivity of O = P(C6Hs)(O-) Radical Anions. *Makromol. Chem.* **1991**, *192*, 2307−2315.
(41) Fairbanks, B. D.; Schwartz, M. P.; Bowman, C. N.; Anseth, K. S. Photoinitiated Polymerization of PEG-Diacrylate with Lithium Phenyl-2, 4, 6- Trimethylbenzoylphosphinate: Polymerization Rate and Cytocompatibility. *Biomaterials* **2009**, *30* (35), 6702−6707.
(42) Franceschi, R. T.; Iyer, B. S. Relationship Between Collagen Synthesis and Expression of the Osteoblast Phenotype in MC3T3-El Cells. *J. Bone Miner. Res.* **1992**, *7* (2), 235−246.
(43) Bhatheja, K.; Field, J. Schwann Cells: Origins and Role in Axonal Maintenance and Regeneration. *Int. J. Biochem. Cell Biol.* **2006**, *38* (12), 1995−1999.
(44) Hudziak, R. M.; Schlessinger, J.; Ullrich, A. Increased Expression of the Putative Growth Factor Receptor P185HER2 Causes Transformation and Tumorigenesis of NIH 3T3 Cells. *Proc. Natl. Acad. Sci. U. S. A.* **1987**, *84* (20), 7159−7163.
(45) Chen, Y.; Wilson, J. A.; Petersen, S. R.; Luong, D.; Sallam, S.; Mao, J.; Wesdemiotis, C.; Becker, M. L. Ring-Opening Copolymerization of Maleic Anhydride with Functional Epoxides: Poly-(Propylene Fumarate) Analogues Capable of Post-Polymerization Modification. *Angew. Chem., Int. Ed.* **2018**, *57*, 12759.
(46) Timmer, M. D.; Jo, S.; Wang, C.; Ambrose, C. G.; Mikos, A. G. Characterization of the Cross-Linked Structure of Fumarate-Based Degradable Polymer Networks. *Macromolecules* **2002**, *35*, 4373−4379.

DOI: 10.1021/acsmacrolett.8b00720
ACS Macro Lett. 2018, 7, 1254−1260